Dynamic Stall on Airfoils Exposed to Constant Pitch-Rate Motion

R.R. Leknys, M. Arjomandi, R.M. Kelso and C. Birzer

School of Mechanical Engineering, the University of Adelaide, Adelaide, South Australia 5005, Australia

Abstract

Gust-like flow behavior is simulated using pitching airfoils to represent the unpredictable nature of atmospheric turbulence on the blades of wind turbines. Angle of attack, reduced frequency and both NACA 0021 and NACA 0012 airfoils are investigated using particle image velocimetry to assess their influence on the developed flow structure resulting from the ramp-up constant angular velocity motion. The pitch motion was shown to delay the onset of the stall vortex to high angles of attack, which is linked to increased lift. Moreover, increasing the reduced frequency reduced the rate of vortex growth as the angle of attack was increased. Development of a rear separation bubble with low velocity is noted during initial development of the dynamic stall process. Once the critical angle of attack is reached, initiation of the formation of the dynamic stall vortex is observed. Increased angular displacement resulted in the annihilation of the trailing edge vortices, by the initial stall vortex, which also coincided with vortex-induced separation leading to bluff body separation. Results from the current work show the presence of delayed separation and vortex formation on the upper surface of the airfoil characteristic to the dynamic stall process. The current work highlights the flow features responsible for enhanced lift, whilst shedding light on the development process for constant-pitch-rate motion about thick and thin airfoil sections.

Introduction

Dynamic stall is the phenomenon of delayed stall whereby large increases in aerodynamic loading are achieved past typical steady state angles of attack. The process of dynamic stall is typically associated with retreating blade stall of helicopters and unsteady atmospheric operation of vertical and horizontal axis wind turbines. For these machines, the additional loading generated by blade pitching leads to excessive fatigue and reduced performance. Furthermore, dynamic stall has been associated with natural flyers including birds and insects where vortex lift is utilised for predatory avoidance, hover and perching manoeuvres [22]. Dynamic stall is characterised by the delay in boundary layer separation followed by the rapid formation of a leading-edge vortex on airfoils undergoing pitching or heaving motions. The delay in boundary layer separation has been attributed to an overall decrease in surface pressure coefficient and delayed collapse of the leading-edge suction peaks resulting in periodic lift generation [8]. Once the leading-edge vortex forms, further lift is generated until the vortex finally departs from the airfoil surface, resulting in deep stall conditions [14].

The awareness of unsteady performance characteristics associated with dynamic stall was first realised through the work of Kramer [9] who identified the additional lift over aircraft wings due to gusts. Proceeding from this initial study and due to the technical advancements of rotorcraft and the requirement for increased speed and manoeuvrability, a wealth of research [2, 3, 11-13, 15] was undertaken to further identify the performance advantages and disadvantages of dynamic stall. Various parametric studies investigating pitch rate, Reynolds number, airfoil geometry and Mach number [4, 6] all seek to identify key performance characteristics associated with each major influencing operating parameter.

Physical parameters that significantly influence the development of dynamic stall include the reduced frequency, $\kappa = \omega C / 2U_\infty$, where ω is the rotation rate in deg/sec taken about the mid-chord location, C is the airfoil chord in meters and U_∞ is the free stream velocity in m/s, other parameters are Reynolds number, Re, based on the airfoil chord; the angle of attack, α; airfoil geometry and non-dimensional pitch location, $\overline{x} = x / C$ where x is the chord-wise location from the leading edge of the airfoil.

Multiple investigations, using surface pressure measurements and smoke-wire flow visualisation, discuss the effects of reduced frequency on dynamic stall [7, 8, 17]. The outcomes of these studies suggest that increasing the reduced frequency leads to the delay in formation of the leading-edge vortex and subsequent enhanced, temporary lift generation. Although reduced frequency has been shown to have a dramatic effect on the development of the dynamic stall and associated forces, research is still required to determine the variations in flow structure across multiple reduced frequencies that are associated with quasi-steady and unsteady flow conditions.

Through the use of surface pressure, [17] conducted systematic studies over Reynolds numbers ranging between 59,000 and 223,000. Decreases in pressure at the leading edge were observed and could be correlated with the formation of a primary and secondary leading edge vortex, however, the development of these structures and overall increase in normal force coefficient was not influenced by Reynolds number. A similar study using surface pressure measurements by Conger and Ramaprian [7], although conducted in a water channel, demonstrates the effects of Reynolds number on a NACA 0015 airfoil undergoing dynamic stall. In this study, the magnitudes of surface pressure peaks were shown to be significantly influenced by the Reynolds number, although the net force coefficient was shown to be minimally affected by variations in Reynolds number. As such, minimal force changes on an airfoil are observed due to the effects of Reynolds number [7, 17, 18]. This suggests that the dynamic stall phenomenon is more sensitive to pitch-induced inertial effects and vortex-induced flows rather than the state of the laminar or turbulent boundary layers.

The above studies were primarily conducted to evaluate the effects of dynamic stall on helicopter rotors where limitations in performance were discovered due to the unsteady flow structures. In recent years, advancements and the urge for cleaner energy production through the application of wind turbines has led to further investigations of dynamic stall [1, 5, 10, 19, 21]. Wind turbine blades are exposed to multiple sources of unsteadiness including atmospheric turbulence, tower shadow and upstream turbulent wakes [10]. The result of these unsteady velocity fluctuation exposes the turbine to dynamic stall conditions. In addition, due to structural and aerodynamic requirements, turbine blade thickness can vary as much as 12% along the total span [20]. Although other performance parameters are heavily investigated, the effects of airfoil geometry have been given less attention. One

comprehensive study [12] investigated eight airfoil sections specific for helicopter applications. This study focused on the effects of dynamic stall with blades thickness ratios varying between 9.5% and 16.5%. In a separate study to overcome performance degradation on wind turbine blades due to leading edge contamination and blade twist, a new family of airfoil profiles was developed specifically for wind turbine applications with thickness ratios varying between 11% and 21% [23]. Although these sections have been utilised in industry, the various aerodynamic properties developed as a result of dynamic stall due to the variation in airfoil thickness has not been fully investigated.

Although the dominating leading-edge vortex is associated with the dynamic stall process, investigation of its development across varying thickness airfoils at extreme angles of attack requires further investigation. The current work sets out to identify the flow structures and velocity variation generated about two symmetrical airfoil geometries with dissimilar thickness ratios relevant to wind turbine operation. Moreover, multiple pitch rates are investigated at extreme angles of attack to establish dynamic-stall conditions.

Experimental Setup

Particle image velocimetry (PIV) was performed in a water channel at the University of Adelaide. A schematic representation of the test apparatus is provided in Figure 1 showing the arrangement of the laser and water channel facility.
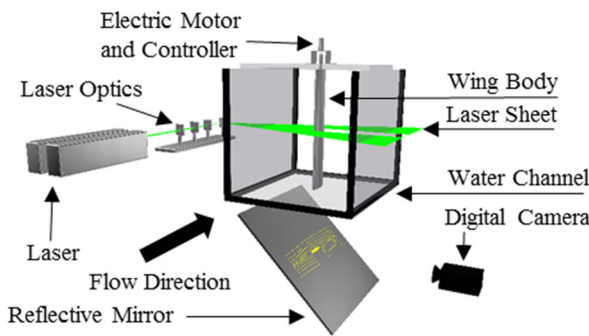
Figure 1. Experimental setup showing the arrangement of the laser, airfoil and camera used for PIV measurements.

A Nd:YAG double-pulsed laser with 532nm wavelength was utilised to create a 3mm thick light sheet for observation of 50μm polyamide seeding particles with a specific gravity of 1.03. Phase-averaged PIV was performed using the combination 200 image pairs of both upper and lower velocity data sets generated, using PIVView V1.7. This provided complete velocity data sets around the airfoil and eliminated shadow created by single-sided evaluation. Constant-pitch-rate motion about the mid-chord location of the wing was supplied via a brushless DC motor with an integrated position encoder and reduction gear box. Reduced frequency values of $\kappa = 0.05, 0.1, 0.2$ were used to simulate quasi-steady and unsteady flows about each of the test airfoils [10]. The airfoil pitch velocity profile was adjusted such that 5° of rotation was allocated for acceleration and deceleration of the test wing with chord, $C = 0.07$m, and span, $S = 0.5$m. Two symmetrical airfoils, with dissimilar thickness ratios, a NACA 0012 and NACA 0021, were selected for testing flow structure development and variation during the dynamic stall process. The water channel velocity was such that a Reynolds number, $Re = 20000$, based on the airfoil characteristic length was achieved.

Quasi-Steady Dynamic Stall

Figure 2 shows the normalised velocity contours and streamline plots of the NACA 0012 and NACA 0021 undergoing dynamic stall between $\alpha = 0° - 60°$ and for a reduced frequency of $\kappa = 0.05$. *For the current flow conditions, quasi-steady conditions are achieved whilst $\kappa = 0.05$.*
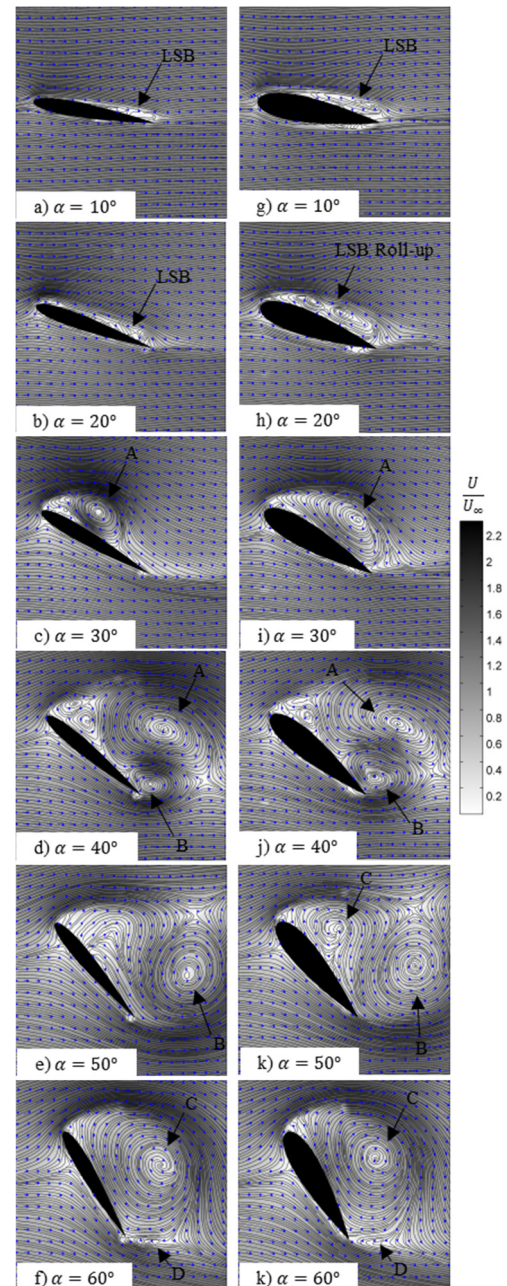
Figure 2. Normalised velocity contours and streamline plots of NACA 0012 (left) and NACA 0021 (right) airfoils undergoing constant-pitch-rate dynamic stall. $\kappa = 0.05$. Shown is the presence of the laminar separation bubble (LSB), leading edge vortex (A), trailing edge vortex (B) and secondary leading edge vortex (C). At this quasi-steady reduced frequency, the airfoil is seen to transition into fully-separated flow at $\alpha = 40°$.

The presence of the laminar separation bubble at the test low Reynolds number is observed in Figure 2(a-b) and Figure 2(g-h) with the leading edge vortex (A) only forming at $\alpha = 30°$ for both airfoils. The laminar separation bubble is shown to be thicker over the NACA 0021, and in addition, the leading edge vortex is shown to form and occupy the total chord length of the airfoil. Comparing this to the NACA 0012 where the leading edge vortex is more defined with higher velocity and only occupies the forward half of the airfoil chord. The presence of a stagnation point at the trailing edge, even after leading edge vortex formation, suggests that the bound circulation continues to grow as a result of vortex generation. Surface pressure measurements in [16] show the

decrease in surface pressure due to the presence of the vortex structures. Also shown in [16] using PIV is the decreased and more intense distribution of surface pressure resulting from a region of high vorticity at the leading edge, compared to a lower broader pressure distribution resulting from a lower vorticity trailing-edge vortex. Relating the flow pattern and surface pressure from [16] to the current work suggests that the NACA 0012 develops a much stronger pressure reduction at the leading edge with comparison to the NACA 0021 where the pressure distribution is expected to be much broader and to a high value. The resulting vortex distribution indicates that for the lower, quasi-steady reduced frequencies, the NACA 0012 will generate a high pitching moment due to the intense vortex adjacent to the forward region of the airfoil. Due to the attachment of the vortex structure, and as suggested in [5], an apparent camber effect and artificial geometry is generated which in addition can be attributed to increased aerodynamic force. The observation of the maximum 'displaced' velocity away from the airfoil boundary itself suggests that an increase in lift is possible even though the boundary layer over the airfoil is seen to break down and form into the dominating vortex structures as indicated in Figure 2c and Figure 2i. Once the leading-edge vortex transitions into the freestream and depart from the surface of both airfoils, as shown from Figure 2d and Figure 2j, initiation of fully-separated flow is achieved. The point at which the leading-edge vortex transitions into the free-stream marks the initiation of deep-stall flow conditions where any further pitching would lead to the formation of a secondary trailing edge vortex (B) and subsequent periodic vortex shedding.

Unsteady Dynamic Stall

For the case of $\kappa = 0.1$, representing unsteady dynamic stall, each of the airfoils was subject to constant-pitch-rate motion to a maximum angle of attack of $\alpha = 60°$. The thickness of the airfoil is shown to directly influence the development of the leading edge vortex in conjunction with the process of laminar separation bubble roll-up on the upper surface of both airfoils. Normalised velocity contours and streamline plots are presented in Figure 3 and can be used to identify the regions of flow separation about both the NACA 0012 and NACA 0021.

As indicated in Figure 3, flow features developed during the pitch-up process are presented and include the laminar separation bubble formed of the upper-rear of the airfoil, as shown in Figure 3(a-b) and Figure 3(g-h) for $\alpha = 10°$ and $\alpha = 20°$. During this period of rotation, the laminar separation bubble is observed to be considerably thinner for the NACA 0012, with comparison to the NACA 0012, whilst the upstream attachment point of the laminar separation bubble is shown to move toward the leading edge until $\alpha = 30°$, Figure 3c, where the formation of the leading edge vortex is observed. At $\alpha = 30°$, the NACA 0021 generates four vortex structures within the laminar separation region whilst the NACA 0012 generates a forward region of vorticity combined with a trailing edge re-circulation zone beginning the process of leading edge vortex formation. Once the leading-edge vortex formed, as shown in Figure 3d and Figure 3j, the effects of flow structure development are seen to become independent of airfoil geometry such that a single leading edge (vortex A) and single trailing edge vortex (vortex B), both of clockwise circulation are formed. In addition, geometry is shown to influence the maximum velocity such that the NACA 0012 generates higher normalised velocity with the leading edge vortex, suggesting that lower pressure coefficients are produced, contributing to high pitching-moment and increased lift compared to the NACA 0021.

Continued rotation results in the amalgamation of the forward two vortex structures and rear vortex structures such that a single dynamic stall vortex (vortex C) exists over the upper surface of the airfoil.
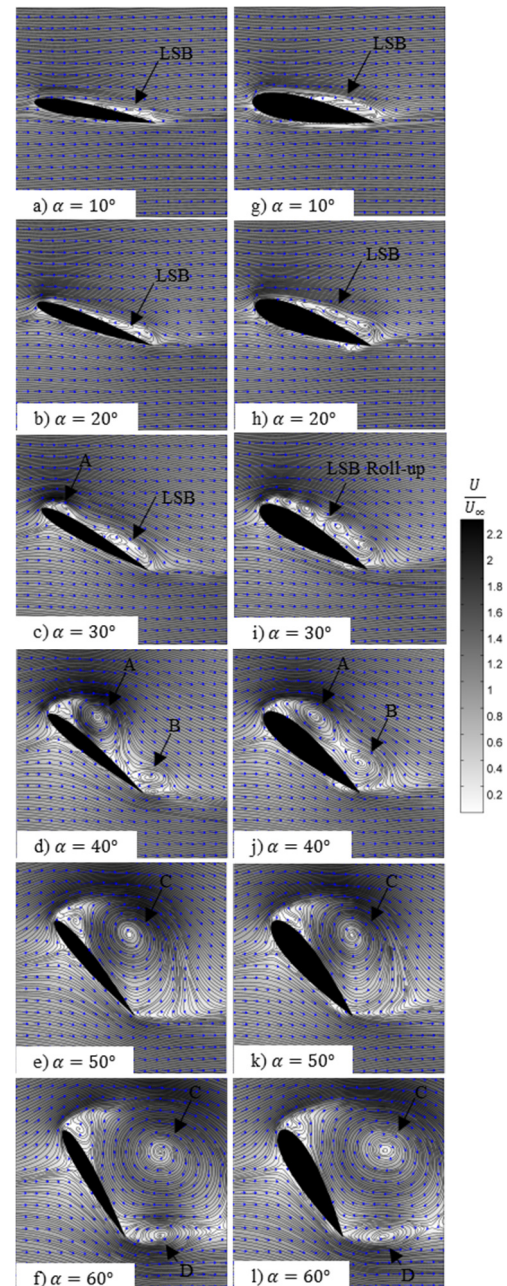
Figure 3. Normalised velocity contours and streamlines of NACA 0012 (left) and NACA 0021 (right) airfoils undergoing constant-pitch-rate dynamic stall. $\kappa = 0.1$. Shown is the presence of the laminar separation bubble (LSB), leading edge vortex (A), counter clock-wise trailing edge vortex (B) and amalgamated leading and trailing edge vortex (C) leading to fully separated flows. A secondary trailing-edge vortex (D) is observed to form as a result of complete stall.

As for the case of the quasi-steady reduced frequency, Figure 2, deep stall is initiated with the presence of a secondary counter-clockwise vortex (vortex D) forming at the trailing edge of both airfoils as indicated in Figure 3f and Figure 3l, suggesting the independence of airfoil geometry with respect to deep stall flow structure. Following $\alpha = 60°$, the airfoil transitions into a phase of fully-separated flow where large-scale bluff body separation in observed.

Leading-Edge Vortex Growth

Growth of the leading edge vortex is shown to be a function of both the maximum angle of attack and the reduced frequency. Figure 4 shows the non-dimensional leading-edge vortex core radius, $\bar{r} = r_{Vort}/C$, as a function of the angle of attack and

reduced frequency where r_{vort} is the leading edge vortex core radius prior to separation from the airfoil. The leading-edge vortex is approximated using the Lamb-Oseen vortex whereby the maximum vortex-core radius can be defined as the radius at which maximum tangential velocity occurs. Results of vortex core radius as functions of angle of attack and reduced frequency as shown in Figure 4. As observed in Figure 4, regardless of the reduced frequency, the airfoil angle of attack allowed for the growth of the leading edge vortex to continue. However, increased reduced frequency is shown not only to delay the formation of the leading edge vortex to higher angles of attack, but also to decrease the rate of vortex growth.
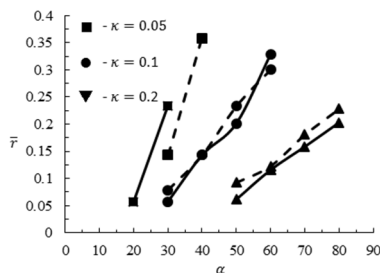
Figure 4. Non-dimensional leading-edge vortex core radius as a function of both angle of attack and reduced frequency. Growth rate is observed to decrease with reduced frequency whilst the onset of vortex formation is delayed. Solid lines represent the NACA 0021 whilst dashed lines represent the NACA 0012.

Conclusion

Flow structure development of the dynamic stall process is presented for unsteady reduced frequencies on multiple airfoils with varying thickness ratios. The thicker airfoil developed broader laminar separation bubble and dynamic stall vortex during reduced frequencies specific to quasi-steady conditions, whilst the thinner airfoil was shown to be more susceptible to abrupt separation resulting in leading edge vortex formation. For unsteady reduced frequencies the flow structure development was similar, although higher velocity gradients were observed about the NACA 0012. Deep stall about both test airfoils was observed to occur once the primary leading-edge vortex transitioned into the free stream and a secondary trailing edge vortex with counter-clockwise circulation was generated. The combination of the attached vortex and airfoil geometry suggests that an artificially-generated profile governs the lift properties of the airfoil due to the additional circulation created by the vortex structure prior to fully separated flow. Observation of velocity contours indicated that the maximum velocity was displaced away from the surface of the airfoil and located between the alleyway separating the leading-edge vortex and the free-stream. Furthermore, increasing the reduced frequency was shown to not only inhibit the initiation of leading edge vortex formation, but it also varied its growth rate where decreased rates of expansion were observed. The developed flow structure and associated forces can be directly related to the unsteady operation of wind turbines, where increased blade fatigue and higher operating costs are incurred, due to the dynamic stall process.

Acknowledgements

References

[1] Butterfield, C.P., A.C. Hansen, D. Simms, and G. Scott, *Dyanamic stall on wind turbine blades,* 1991, National Renewable Energy Laboratory.

[2] Carr, L.W., Progress in analysis and prediction of dynamic stall. *Journal of Aircraft*, 1988. **25**(1): p. 6-17.

[3] Carr, L.W., K.W. McAlister, and W.J. McCroskey, Analysis of the development of dynamic stall based on oscillating airfoil experiments. 1977.

[4] Chandrasekhara, M., M. Wilder, and L. Carr, Boundary-layer-tripping studies of compressible dynamic stall flow. *AIAA Journal*, 1996. **34**(1): p. 96-103.

[5] Choudhry, A., R. Leknys, M. Arjomandi, and R. Kelso, An insight into the dynamic stall lift characteristics. *Experimental Thermal and Fluid Science*, 2014. **58**: p. 188-208.

[6] Choughuri, P.G. and D.D. Knight, Effects of compressibility, pitch rate, and reynolds number on unsteady incipient leading-edge boundary layer separation over a pitching airfoil. *Journal of Fluid Mechanics*, 1996. **308**: p. 195-217.

[7] Conger, R.N. and B.R. Ramaprian, Pressure measurements on a pitching airfoil in a water channel. *AIAA Journal*, 1994. **32**(1): p. 108-115.

[8] Jumper, E.J., S.J. Schreck, and R.L. Dimmick, Lift-curve characteristics for an airfoil pitching at constant rate. *Journal of Aircraft*, 1987. **24**(10): p. 680-687.

[9] Kramer, M., Increase in the Maximum Lift of an Airplane Wing due to a Sudden Increase in its Effective Angle of Attack Resulting from a Gust. 1932.

[10] Leishman, J.G., *Principles of helicopter aerodynamics*. 2 ed. 2000, New York: Cambridge Aerospace Press.

[11] McAlister, K.W. and L.W. Carr, Water tunnel visualisations of dynamic stall. *Journal of Fluids Engineering*, 1979. **101**(3): p. 376-380.

[12] McCroskey, W., K. McAlister, L. Carr, and S. Pucci, An experimental study of dynamic stall on advanced airfoil sections. Volume 1: Summary of the experiment. 1982.

[13] McCroskey, W., K. McAlister, L. Carr, S. Pucci, O. Lambert, and R. Indergrand, Dynamic stall on advanced airfoil sections. *Journal of the American Helicopter Society*, 1981. **26**(3): p. 40-50.

[14] McCroskey, W.J., *The phenomenon of dynamic stall,* 1981, DTIC Document.

[15] McCroskey, W.J., L.W. Carr, and K.W. McAlister, Dynamic stall experiments on oscillating airfoils. *Aiaa Journal*, 1976. **14**(1): p. 57-63.

[16] Mueller-Vahl, H., C. Strangfeld, C.N. Nayeri, C.O. Paschereit, and D. Greenblatt, *Thick Airfoil Deep Dynamic Stall*, in *Wind Energy-Impact of Turbulence*. 2014, Springer. p. 35-40.

[17] Robinson, M.C. and J.B. Wissler, Pitch rate and Reynolds number effects on a pitching rectangular wing. *AIAA Journal*, 1988. **88**: p. 2577.

[18] Schreck, S.J., W.E. Faller, and H.E. Helin, Pitch rate and Reynolds number effects on unsteady boundary-layer transition and separation. *Journal of Aircraft*, 1998. **35**(1): p. 46-52.

[19] Schreck, S.J., M.C. Robinson, M. Maureen Hand, and D. Simms, A, Blade dynamic stall vortex kinematics for a horizontal axis wind turbine in yawed conditions. *Journal of Solar Energy Engineering*, 2001. **123**(4): p. 272-281.

[20] Schubel, P.J. and R.J. Crossley, Wind turbine blade design. *Energies*, 2012. **5**(9): p. 3425-3449.

[21] Shipley, D.E., M.S. Miller, and M.C. Robinson, *Dynamic stall occurance on a horizontal axis wind turbine,* 1995, National Renewable Energy Laboratory.

[22] Shyy, W., Y. Lian, J. Tang, D. Viieru, and H. Liu, *Aerodynamics of low reynolds number flyers*. Vol. 22. 2007: Cambridge University Press.

[23] Tangler, J.L. and D.M. Somers, *NREL airfoil families for HAWTs*. 1995: Citeseer.